Neutron scattering study of ^{36}Ar monolayer films adsorbed on graphite

H. Taub,* K. Carneiro,† J. K. Kjems,‡ and L. Passell
Brookhaven National Laboratory,§ Upton, New York 11973

J. P. McTague‖
University of California, Los Angeles, California 90024

(Received 28 June 1977)

Diffraction of neutrons from ^{36}Ar monolayers adsorbed on graphite basal planes indicates that an ordered, two-dimensional (2D) triangular lattice is formed at low temperature. The lattice constant is found to be slightly larger than that of the bulk 3D solid but significantly smaller than that of a registered $\sqrt{3}\times\sqrt{3}$ overlayer. Thermal expansion of the monolayer is anomalously large; up to 60 K the linear expansion is 4.5 times greater than in the 3D solid. There is no evidence of a sharp melting transition. Instead, the positional correlations (which extend to the full dimensions of the crystallite surfaces at low temperatures) are observed to decrease smoothly above 40 K, falling from 100 to 15 Å at 80 K. Little if any positional order remains at temperatures where the nearest-neighbor distance in the monolayer matches that of a registered $\sqrt{3}\times\sqrt{3}$ phase. The spectrum of neutrons inelastically scattered from ^{36}Ar monolayers in the nominally in-plane configuration can be reasonably well described at low temperatures by a 2D harmonic-phonon model while the scattering in the out-of-plane configuration seems to be best represented in terms of a resonant coupling of the monolayer film to out-of-plane collective motions of the graphite substrate. There is some evidence of renormalization of the in-plane transverse modes of the monolayer at higher temperatures; however, the in-plane longitudinal modes and the out-of-plane modes do not appear to be similarly affected.

I. INTRODUCTION

New spectroscopic methods of probing surfaces have had a revolutionary impact on surface science. Particularly where chemisorbed phases are concerned, the introduction of microscopic techniques has made possible the investigation of such things as the structures of the surface films, the site specificity of binding and the electronic rearrangements associated with the formation of surface bonds. Information so developed has led to notable advances in the basic understanding of chemisorbed species.

Although physisorption is a much simpler process than chemisorption, it has not been as well explored experimentally. Primarily this is because of the weakness of the electrostatic (Van der Waals) bond which couples physisorbed atoms to surfaces. Almost without exception, the spectroscopic probes used to study chemisorbed phases are too disruptive to be applied to any but the most tightly bound physisorbed systems. As a consequence, very little is known about weakly bound films beyond what can be deduced from thermodynamic investigations.[1] One particularly striking feature is revealed by these experiments: on uniform surfaces, physisorbed films form well-defined monolayers which are capable of undergoing changes of phase analagous to those occuring in bulk matter. Much has been conjectured concerning the types of phase transitions taking place in the films, the nature of the phases involved, and the possible relationships between weakly bound surface monolayers and the idealized two-dimensional (2D) systems of theory. But, in the absence of spectroscopic information, there has been no clear-cut way to interpret bulk experiments on physisorbed phases in microscopic terms.

Among the probes currently employed for studies of condensed matter, none causes less disruption of the system under examination than the neutron. Accordingly, we began some time ago to use neutrons to investigate the microscopic properties of weakly bound surface films. Thus far, we have applied the technique to three such systems: N_2,[2] ^{36}Ar,[3] and ^{4}He (Ref. 4) absorbed on Grafoil,[5] an exfoliated graphite foil with remarkably uniform surfaces which is widely used as a substrate for thermodynamic investigations. Others active in this field have used neutrons to study hydrogen and deuterium,[6,7] oxygen,[8] and krypton[9] on Grafoil and there are also reports in the literature describing neutron experiments with hydrogenous materials absorbed on a number of high-surface-area substrates.[10-13]

Marginal scattered intensities forced us to limit our investigations of N_2 and He monolayers to study of the elastic diffraction alone. But since ^{36}Ar is a much more effective coherent scatterer of neutrons than either N_2 or He, it proved possible in this case to investigate both the inelastic and elastic components of the scattering. Reference 3 contained only a brief, preliminary account of these experiments. Our intention here is to describe them at greater length and to discuss their interpretation in more detail.

In treating physisorbed monolayers theoretically, it has generally been the practice to consider them as 2D entities and to represent the bonds between atoms and those to the substrate by simple interaction potentials. One of the primary objectives of this study was to see how well such models describe the behavior of a real film on the most uniform surface currently available. To do this in a reasonably definitive way required investigation of both the structure and the dynamical response of the adsorbed Ar layers. As will soon be evident, although the structures of the films were relatively easy to determine, the polycrystalline nature of the substrate made the dynamical response much more of a problem to resolve. Nevertheless, by using a computer to model the interaction of neutrons with the excitations of the film we found it was still possible to extract a considerable amount of dynamical information from our measurements.

II. EXPERIMENTAL TECHNIQUES FOR PHYSISORPTION STUDIES

A. Thermodynamic methods

As noted, the greatest part of what is presently known about physisorbed phases comes from thermodynamic studies, most often heat-capacity or adsorption-isotherm measurements. Probably the most comprehensive bulk studies are those concerned with He adsorbed on the basal plane surfaces of Grafoil.[14,15] Along with limited structural information, these experiments give an indication of the velocities of longitudinal and transverse sound modes propagating in the films. Significantly, it is found that He monolayers at low temperatures are able to support transverse shear waves, one of the identifying features of a solid.

Among the more classical systems, investigations of the adsorption isotherms of Kr,[16,17] Xe,[18] and[19] Ar on exfoliated graphite should be mentioned because of their close relationship to our measurements. In addition, there are reports in the literature describing studies of the heat capacity of Ar on both Graphon[20] and graphitized carbon black[21] at a variety of coverages. Particularly relevant is the data of Ref. 21 showing a pronounced peak in the heat capacity of 0.5 monolayer Ar films at a temperature of 67 K. It is thought that this peak is associated with some type of 2D phase transition.

B. Microscopic probes

1. Electron spectroscopy

Chemisorbed films are now routinely investigated with various forms of electron spectroscopy. The best-known and most widely applied techniques are low-energy-electron diffraction (LEED), x-ray photoelectron spectroscopy (ESCA), and Auger spectroscopy.[22] In general, electrons probe only atoms near or on the surface and in cases where the sample is an insulator, the surface layer is usually ionized to some extent by the interaction process.

Electron spectroscopy has not been notably successful to date when applied to physisorbed films. With these films, adsorption energies are typically only 0.1 or 0.2 eV and, as a consequence, at all but the lowest temperatures there is a significant concentration of vapor above the substrate surface which scatters the beam. Furthermore, ionization and local heating at the surface is often sufficient to disturb the more weakly bound films.[23] Nevertheless, both LEED and Auger spectroscopy have been applied at low temperatures to the study of selected physisorbed phases. Probably the best example is Xe adsorbed on the basal-plane surface of graphite. LEED data[24,25] indicate that a $\sqrt{3} \times \sqrt{3}$ epitaxial structure is formed at monolayer coverages. In addition a certain amount of dynamical information is obtained in the form of temperature dependent Debye-Waller factors,[26] but by and large, the energy-resolution requirements are too stringent to make electron spectroscopy very useful for dynamical studies.

2. Nuclear magnetic resonance

NMR spectroscopy has been employed to some extent in the high temperature fluidlike regime to examine the diffusive motions of adsorbed atoms and molecules. Among other systems, it has been applied to ethyl alcohol on Grafoil[27] and to ^{3}He on graphitized carbon black[28] and Grafoil.[29,30]

3. Neutron scattering

Neutrons are widely used to investigate the structure and dynamics of bulk liquids and solids where they are acknowledged to be the most versatile probe currently available. Their application to surface studies has, however, been very limited to date. The reasons for this were discussed at length in Ref. 2 and need not be considered in detail here. Briefly, the problem is that unlike strongly interacting charged particles, neutrons are not preferentially scattered by surface layers. To obtain the necessary discrimination against background scattering from the substrate (which constitutes the bulk of the sample) it is therefore necessary to choose systems composed of adsorbates with relatively large coherent scattering cross sections deposited on large surface area substrates with capture and scattering cross sections small enough to make them reasonably transparent to neutrons.

For inelastic processes (which are notably

weaker than elastic processes) the problem becomes even more serious. Fortunately, some improvement in background discrimination is normally associated with inelastic scattering from surface films. Basically, this is because the collective modes of weakly bound films will generally have lower energies than the equivalent modes of the more rigid substrate. Furthermore, the neutron interaction cross section increases with decreasing phonon energy giving added weight to inelastic scattering from the film. And, sometimes in special cases, further improvement in background discrimination can be obtained by selecting films composed of lighter atoms (which are more effective as inelastic scatterers because the inelastic cross sections varies inversely with the mass of the scatterer) on substrates of heavier atoms, which—other things being equal—will scatter less effectively.

All of our work to date on adsorbed phases has involved the use of Grafoil as a substrate. As we mentioned, Grafoil is a popular choice for thermodynamics studies because of its nearly ideal surfaces. Remarkably, it is also an excellent material for neutron investigations. In part is this be- of the quality of its surfaces, but there are other reasons as well. These include the fact that Grafoil offers large specific areas, is relatively transparent to neutrons and has a high atomic density in the basal planes which serve as adsorption surfaces. For the latter reason, the background due to (hk0) diffraction peaks from the substrate is in general well separated from peaks produced by the lower density overlayer films. An added attraction of Grafoil is that it has considerable basal plane orientational order which allows the scattering to be partly decomposed into in-plane and out-of-plane components. And finally, it should be noted that the dynamical response of all forms of graphite is predominantly at energies higher than that of typical surface films—an important feature for inelastic investigations.

III. EXPERIMENTAL APPARATUS AND PROCEDURES

A. Sample cell, gas handling, cryogenics, and thermometry

For most of these measurements we used a slightly modified version of the sample cell employed for the N_2 studies described in Ref. 2. The new cell was of the same diameter as the old one (44 mm) but was made shorter to allow its orientation to be varied within the restricted volume of the cryostat. It was filled with ^{36}Ar from a closed gas-handling system, connection being made via a Cu-Ni capillary. To precisely define the amounts of gas added, we used PVT measurements; these were performed at room temperature with calibrated volumes and a calibrated Bourdon-type pressure gauge. Adjustments for the amount of gas present as vapor were made as necessary to maintain a fixed quantity of ^{36}Ar in the adsorbed phase; the adjustments were based on the known volumes (warm and cold) in the system and on the measured vapor pressure. Typically, about $\frac{1}{2}$ l (STP) of ^{36}Ar gas was required to obtain one monolayer coverage.

The cell itself was mounted in a variable-temperature helium cryostat operating between 4.5 K and room temperature. All temperature measurements were made with calibrated germanium and platinum-resistance thermometers embedded in the copper-heat exchanger block of the cryostat.

B. Grafoil substrate

The shortened cell contained 50 g of Grade GtA Grafoil, slightly more than 0.8 of the amount used for our nitrogen measurements. For this amount of Grafoil the effective surface area is about 1400 m^2 (estimated from the registered $\sqrt{3} \times \sqrt{3}$ phase of nitrogen). Figure 1 shows the measured adsorption isotherms of Ar and N_2 in our cell—the latter scaled to the reduced quantity of Grafoil. Note that the first knee in the Ar isotherm occurs at a higher coverage indicating that Ar forms a denser monolayer phase than N_2.

Apart from knowledge of the effective area, it is also essential for analysis of the data to be able to characterize the size, shape and orientational distribution of the graphite crystallites of which Grafoil is composed. The methods employed to do this were described in Ref. 2 but since the results will be needed in the discussion to follow we will review them briefly. From the natural width of the {002} graphite diffraction peak as observed in the

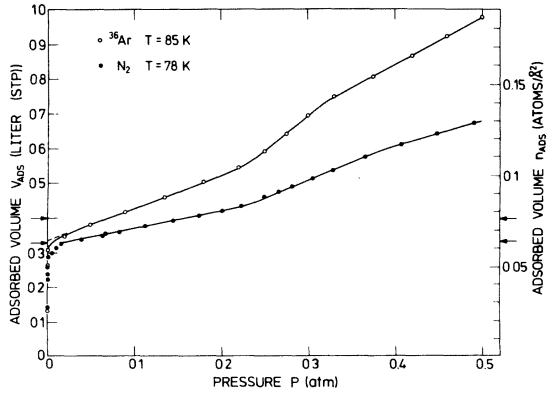

FIG. 1. Adsorption isotherms of ^{36}Ar and N_2 on Grafoil as observed in the sample cell used for these experiments. The arrows indicate monolayer coverage at low temperature. Note that Ar forms a denser monolayer phase.

out-of-plane geometry we estimated the average thickness of a graphite crystallite along the c-axis direction to be about 110 Å corresponding to roughly 33 planes of carbon atoms. The average basal-plane dimension of a crystallite was less easily determined because none of the ($hk0$) diffraction peaks are well separated in the graphite diffraction pattern. But what is actually relevant here is not so much the crystallite dimension as the effective dimension of the adsorbed film on its basal plane surfaces. This can be estimated from the width of the leading edge of the low-temperature adsorbed-phase diffraction peak; for the gases studied to date the effective size of the film is never much greater than 100 Å. This may be a measure of the average dimension of a crystallite surface, however, it could equally well be regarded as an indication of the average distance between surface irregularities, such as steps, which limit the size of the adsorbed films.

Even more important than the effective dimensions of the crystallites is knowledge of their orientational distribution. This can be determined from the rocking curve of the {002} reflection; in Grafoil the crystallite c axes are found to point preferentially normal to the foil planes, the distribution having a full width at half-maximum of about 30°. But as was the case with the surface dimension, what is actually essential is not the orientational distribution of (002) planes but rather that of the adsorbing surfaces. Analysis of the shapes of diffraction peaks from adsorbed films indicates that the surfaces are more isotropically distributed than the (002) planes, presumably because the smaller less-well-oriented crystallites have larger surface to volume ratios and therefore provide proportionally more of the surface area. In Ref. 2 the orientational distribution was described in terms of a function of the form

$$H(\gamma) = H_0 + H_1 \exp[-\tfrac{1}{2}(\gamma/\delta)^2], \quad (1)$$

γ being the angle between a particular adsorbing surface and the foil plane and δ an effective mosaic parameter for the partially oriented crystallites. The first term represents the purely isotropic part of the distribution and the second the partially oriented part. As was explained in Ref. 2, the parameters of Eq. (1) were obtained by fitting a theoretical line shape to the trailing edge of the $\sqrt{3} \times \sqrt{3}$ registered phase diffraction peak from adsorbed N_2, it being assumed that the effect of the Debye-Waller factor on the registered phase line shape would be negligible at low temperatures. Figure 2(a) shows the resulting orientation distribution.

Although Grafoil is evidently not a highly ordered material, it still provides some preferential coupling of the scattering to atomic correlations (both static and dynamic) either in or normal to the adsorbed film planes. Defining the scattering vector $\vec{Q} = \vec{k}_i - \vec{k}_f$, where $\vec{k}_i$ and $\vec{k}_f$ are the incident and scattered neutron wave vectors respectively, it is easy to see from Figure 2(b) that positioning the sample so that $\vec{Q}$ is parallel to the foil planes (i.e., normal to the most probable lattice vector $\vec{c}$) emphasizes the in-plane part of the scattering while $\vec{Q}$ perpendicular to the foil planes emphasizes the out-of-plane component. Intermediate positions alter the relative weightings; however, neither component can be completely isolated from the other by sample orientation alone. But as we will show, model calculations incorporating the orientational distribution of the adsorbing surfaces can be used to simulate the scattering with different cell orientations and these will (within certain limits) provide a method of decomposing the observed spectra into in-plane and out-of-plane components.

C. Neutron spectroscopy

All measurements were made on a triple-axis neutron spectrometer using a fixed incident neutron wavelength $\lambda = 2.5$ Å. Both the monochromating and analyzing crystals were pyrolytic graphite. Higher orders reflected from the monochromator were removed from the incident beam with pyrolytic graphite filters. Horizontal collimation throughout was fixed at 40′ of arc [full width of half-maximum (FWHM)]; vertical at about one degree.

Elastic diffraction scans were made in the triple-axis mode with the analyzer set to accept only elastically scattered neutrons. The inelastic scans were made in the constant-$\vec{Q}$ mode, primarly with neutron energy loss.

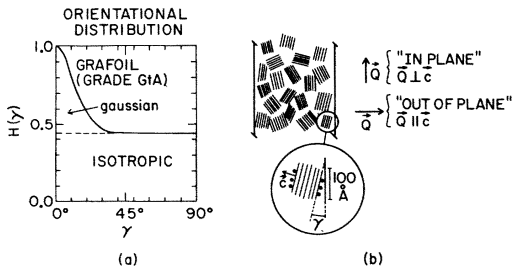

FIG. 2. (a) The orientational distribution of crystallite surfaces in Grafoil as derived from analysis of the diffraction profile of N_2 adsorbed as a registered $\sqrt{3} \times \sqrt{3}$ phase. (b) Relationship of the "in-plane" and "out-of-plane" scattering geometries to the orientational distribution of crystallites in a Grafoil sheet.

IV. ELASTIC DIFFRACTION SCATTERING FROM THE ADSORBED ARGON FILMS

A. Structure of the ^{36}Ar monolayer

Measuring diffraction scattering from adsorbed films is a two-step process. First, a series of background scans is made with no gas in the cell. Afterwards, the cell is filled with gas and the sequence repeated. The scattering from the films is taken to be the difference in counts between the filled and empty cell.

In this particular series of experiments, backgrounds were measured at 20-K temperature intervals from 4.5 to 80 K. Figure 3 shows typical data both with and without gas in the cell. The background (the dashed line in the figure) contains a broad {002} reflection at $Q = 4\pi \sin\Theta/\lambda = 1.87$ Å^{-1} due to misaligned graphite crystallites with c-axes parallel to the foil planes. There are also unresolved background peaks near 3 Å^{-1} associated with the {100}, {101}, and {102} graphite reflections as well as weak reflections from the aluminum walls of the sample cell.

Figure 4(a) shows examples of typical ^{36}Ar difference diffraction patterns observed at low temperatures. Three diffraction peaks appear in the scan; all have "sawtooth" profiles—the identifying characteristic of diffraction from disoriented 2D arrays. The reasons for this asymmetric shape were first investigated by Warren[30] who considered the scattering of x rays from 2D structures and derived an expression for diffraction from a randomly oriented array of finite-sized 2D crystallites. With some minor modifications Warren's line-shape calculation also applies to the neutron case. We will not attempt to discuss it in detail here but will simply quote the relevant expression. Further information can be obtained from Ref. 2 and from Warren's original paper. For a spatially random array of 2D crystallites, the intensity diffracted at an angle 2Θ by the hk Bragg reflection is found to be of the form

$$I_{hk} = N \frac{m_{hk} |F_{hk}|^2 f^2(\Theta) e^{-2W}}{(\sin\Theta)^{3/2}} \left(\frac{L}{\pi^{1/2}\lambda} \right)^{1/2} \mathfrak{F}(a) . \quad (2)$$

In this expression, N is an over-all normalization constant, m_{hk} identifies the multiplicity of the hk reflection, F_{hk} represents the crystal structure factor, $f(\Theta)$ is the molecular form factor, e^{-2W} is the Debye-Waller factor, and

$$\mathfrak{F}(a) \equiv \int_0^\infty e^{-(x^2-a)^2} dx , \quad (3)$$

where $a = (2\pi^{1/2}L/\lambda)(\sin\Theta - \sin\Theta_{hk})$ and $\Theta_{hk} = \sin^{-1}\lambda/2d_{hk}$, λ being the wavelength and d_{hk} the 2D "plane spacing" for the hk reflection. L is a parameter defining the average size of the diffracting arrays. If Eq. (2) were to be plotted for given values of L, λ, and d_{hk} it would show a rising leading edge with a width determined by L, a maximum at

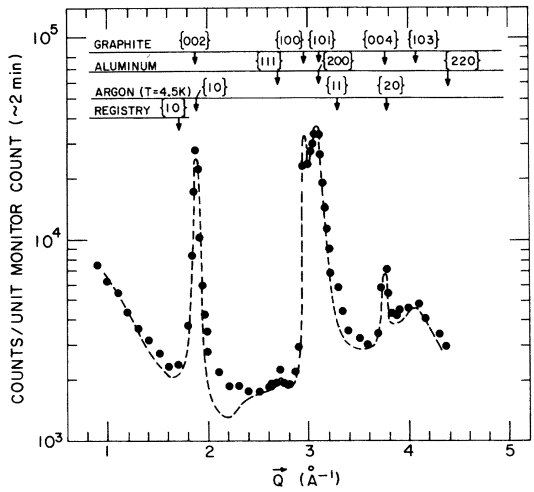

FIG. 3. Diffractions scans at $T = 4.7$ K with the scattering vector $\vec{Q}$ parallel to the foil planes. The dashed line represents the diffraction profile with only Grafoil in the cell, the solid circles show the additional scattering when a monolayer of ^{36}Ar is added. The arrows at the top identify the positions of diffraction peaks.

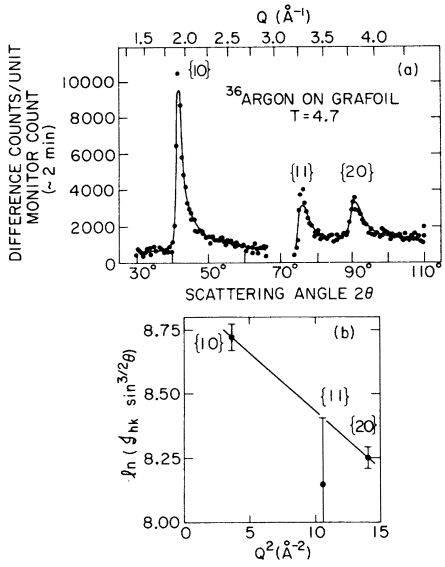

FIG. 4. (a) Difference diffraction pattern from the ^{36}Ar monolayer showing the {10}, {11}, and {20} peaks from the film. The solid lines are fits of the individual peaks to Eq. (4). (b) Q^2 variation of the logarithm of the product of the peak intensities and $(\sin\theta)^{3/2}$. The estimate $\langle u_{10}^2 \rangle = 0.04$ Å^2 is based on the straight line fitted to the {10} and {20} data.

essentially $2\Theta_{hk}$ coming from 2D crystallites with planes parallel to the scattering plane and, finally, an extended trailing edge due to diffraction from the projection onto the scattering plane of the repeat distances of misoriented crystallites. As it stands, however, Eq. (2) cannot be directly applied to experimental data because it does not take into account either the finite resolution of the spectrometer or preferred orientation among the diffracting arrays. When these effects are included, the expression for the line shape assumes the form

$$g_{hk}(\Theta) = \int R(\Theta - \Theta')H[\gamma(\Theta')]I_{hk}(\Theta')\,d\Theta' , \qquad (4)$$

where $R(\Theta)$ represents the instrumental resolution function (see Ref. 2), $H[\gamma(\Theta)]$ the orientational distribution function defined in Eq. (1) above and I_{hk} is defined by Eq. (2).

In fitting Eq. (4) to the observed diffraction profiles from ^{36}Ar films, the parameters of the instrumental resolution function $R(\Theta)$ and the orientational distribution function $H[\gamma(\Theta)]$ were kept fixed at the values obtained from analysis of the adsorbed N_2 films (Ref. 2). Since we were dealing with monolayer and submonolayer films in which there is only one Ar atom per unit cell the structure factor in Eq. (2) was always set equal to unity. The molecular form factor $f(\Theta)$ and m_{hk} were also set equal to unity; the former because argon is a monatomic gas and the latter because all reflections accessible to investigation had the same multiplicity. Thus the only undetermined parameters in the analysis were the 2D plane spacings d_{hk}, the size (or correlation range) parameter L and the argument of the Debye-Waller factor, i.e., $2W(Q) = \langle(\vec{Q}\cdot\vec{u})^2\rangle$, where $\vec{u}$ represents the vector displacement of an atom from its equilibrium position and the angular brackets denote an ensemble average. Of the unknown quantities, d_{hk} is effectively determined by the positions of the diffraction peaks, L by the intrinsic widths of their leading edges, and $2W$ by the relative intensities of the peaks and the shapes of their trailing edges.

When the diffraction profiles of Fig. 4(a) were individually fitted to Eq. (4), we found that they could be indexed as {10}, {11}, and {20} reflections from a triangular lattice with a nearest-neighbor distance $a_{nn} = 3.86$ Å. Figure 5 shows a representation of this lattice which is the closest packing arrangement in two dimensions. Clearly the periodicity of the film is incommensurate with that of the underlying graphite basal plane, the nn distance being 10% smaller than 4.26 Å, the equivalent distance for an epitaxial $\sqrt{3} \times \sqrt{3}$ overlayer. But if we compute the quantity $2^{1/6}\sigma$ (the equilibrium distance between classical Lennard-Jones particles) using for σ the value 3.40 Å obtained from virial coefficient studies of Ar gas,[31] we find $a_{nn} = 3.82$ Å, very close to the value observed in both the surface Ar monolayer and the bulk solid phase.[32] There seems to be little doubt that the structure of the film is primarily determined by the couplings between Ar atoms; in this case at least, interactions with the substrate appear to play at most a secondary role. In fact we were unable to find a combination of coverage and temperature at which an epitaxial $\sqrt{3} \times \sqrt{3}$ ordered phase could be positively identified. This is in sharp contrast to adsorbed N_2 which forms a $\sqrt{3} \times \sqrt{3}$ 2D solid phase at monolayer coverages and below.

As was mentioned, the size parameter L is determined from the width of the leading edge of the diffraction peak. From the profiles of Fig. 4(a) and similar low-temperature data we found $L \sim 105$ Å, essentially the same value as that obtained from equivalent studies of adsorbed N_2. We infer from this that the size of the 2D Ar arrays is limited by the effective dimensions of the graphite surfaces, not by any intrinsic property of the films themselves.

We also attempted to obtain a value for the Debye-Waller factor which gives us information about atomic displacements in the film. Usually these displacements are isotropic or nearly so and according to Eq. (2) we should expect to be able to determine the mag-

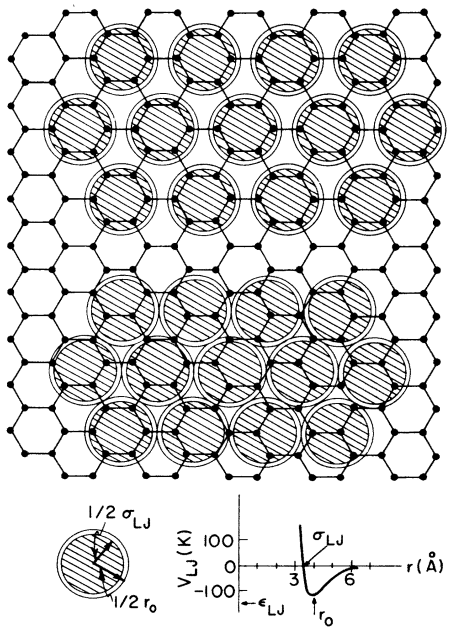

FIG. 5. Schematic representation of the $\sqrt{3} \times \sqrt{3}$ registered phase (top) and of the incommensurate Ar monolayer phase (middle). The Ar-Ar Lennard-Jones potential obtained from gas phase studies is plotted at the bottom.

nitude of $2W(Q)$ by simply plotting the quantity $\ln[\mathcal{I}(\Theta_{hk})(\sin\Theta)^{3/2}]$ against Q^2. Unfortunately, this approach led us into difficulty when we applied it to the observed diffraction peaks. As is evident in Fig. 4(b) the {11} intensity appears to be low compared to that observed for the {10} and {20} reflections. It may be that the low {11} intensity is due to an error in determining the relatively large background contribution from the nearby graphite {101} peak. But an alternative explanation must also be considered; namely that the monolayer takes up a fixed orientation on the substrate surface and the low {11} intensity is thus an indication of static strains in the film along the {11} direction produced by the incommensurate periodicity of the underlying graphite lattice. This can be ruled out, however, because investigation shows that the sixfold symmetry of the monolayer-substrate system requires that all strains be isotropic. About all that can be said with confidence is that the Q dependence of the {10} and {20} intensities indicates that $\langle u_{10}^2\rangle \sim 0.04$ Å^2, a value which may include both static and dynamic contributions.

Before leaving the subject of atomic displacements a few words should also be said about estimating the Debye-Waller factor from its influence on the shape of the trailing edges of the 2D diffraction peaks. While this is possible in principle, we have found that in practice it requires a more precise knowledge of the orientational distribution of substrate surfaces than we have at the present time. In such circumstances we do not feel that this procedure represents a viable alternative to the standard approach outlined above.

B. Thermal effects on film structure

The fact that monolayer Ar films are not in registry implies that they are little affected by the spatial periodicity of the substrate potential and might therefore be expected to exhibit some of the characteristics of idealized 2D systems. Some years ago Peierls[33] and Mermin[34] showed that such systems are not expected to develop true long range positional order at finite temperatures. The essential point of their argument can be grasped by considering a simple example, namely a 2D Debye solid. In this case

$$\langle u^2\rangle \simeq \int_{\pi/L}^{\pi/a} \langle u_q^2\rangle q\,dq \int_{\pi/L}^{\pi/a} q\,dq\,, \tag{5}$$

where a is the lattice parameter and L the dimension of the crystal. Now

$$E_q = k_B T = m\omega^2\langle u_q^2\rangle = mv_0^2 q^2\langle u_q^2\rangle\,, \tag{6}$$

v_0 being the velocity of sound. Substituting from Eq. (6) into (5) results in the relation

$$\langle u^2\rangle \approx \int_{\pi/L}^{\pi/a} q\,\frac{k_B T}{mv_0^2}\,\frac{1}{q^2}\,dq \approx \frac{a^2 k_B T}{\pi^2 m v_0^2}\ln(L/a)\,, \tag{7}$$

i.e., $\langle u^2\rangle$ is seen to diverge logarithmically with argument L/a. But it is easy to show by using reasonable values for the sound velocity and temperature that the quantity $k_B T/\pi^2 m v_0^2$ will be of magnitude 10^{-3}. Furthermore, with Grafoil as a substrate L/a is unlikely to exceed 25. Consequently for the films of interest here the logarithmic divergence can hardly be expected to have any significant effect on the range of order. Nevertheless, its existence suggests that thermal influences on 2D and 3D systems could be significantly different, even when the former are not of large size.[35]

With this in mind we turn to consideration of the thermal expansion of the adsorbed ^{36}Ar films. Figure 6 shows the temperature dependence of the nearest-neighbor distance a_{nn} as deduced from the position of the {10} diffraction peak. Total linear expansion in the film up to 60 K is 9%, the most rapid change taking place between 40 and 60 K. Solid argon by comparison shows a linear expansion of only 2% over the same temperature interval. Note that nowhere in the temperature range studied is there any evidence of an abrupt change in the film density such as normally occurs at melting.

The shapes of the diffraction peaks also fail to show any indication of a sudden phase transition. What happens at higher temperatures is simply that the peak intensity continuously decreases (see Fig.

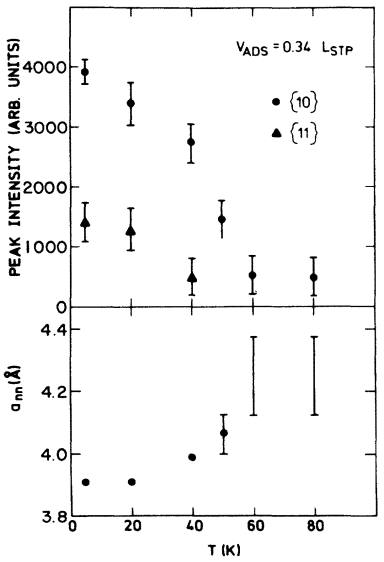

FIG. 6. Temperature variation of the intensities of the {10} and {11} diffraction peaks (top) and of the nearest-neighbor distance (bottom) in the Ar monolayer. The diffraction peaks were too broad to permit the nearest-neighbor distance to be clearly defined above 60 K.

6) and its leading edge broadens indicative of a decrease in either the range of order or alternatively of the size of the diffracting arrays. Plotted in Fig. 7 is the temperature dependence of the size parameter L (possibly better regarded in this context as a measure of the positional correlation range) together with equivalent data for the registered phase of adsorbed N_2. At temperatures above 40 K L decreases smoothly; in fact it varies with temperature approximately as $\exp(-T/T_0)$ with $T_0 = 25$ K. We already remarked on the fact that there is no abrupt change in the lattice constant as these films are heated. Thus neither the positional order nor the density of the monolayer shows evidence of the discontinuous changes usually associated with the melting of bulk solids. In striking contrast to this, the registered N_2 phase appears to maintain the imposed long-range order of the graphite substrate until it melts abruptly near 70 K.

One cannot, of course, completely rule out the possibility of a sharp phase transition just because there are no sudden changes in either the positional correlations or the density. But it is at least clear from our observations that if there is a sharp melting transition in adsorbed Ar monolayers, neither the difference between solid and liquid densities nor the correlation range is the relevant order parameter.

There are both theoretical analyses[36] and computer simulations[37] of 2D melting which suggest that the process proceeds via the cooperative production of dislocations. The appearance of dislocations is thought to cause softening of the transverse modes and ultimately a loss of resistance to shear. In the Kosterlitz-Thouless-Feynman dislocation picture,[15,36] the melting temperature is expressed as

$$T_m \approx \frac{mk_B}{32\pi^2\hbar^2} a_{nn}^2 \Theta_{2D}^2 , \tag{8}$$

where Θ_{2D} represents the Debye temperature of the 2D solid. If we arbitrarily define the melting temperature of the Ar monolayer as the point where L is halfway between its ordered and disordered limits, then $T_m \approx 50$ K and from Eq. (8) we find $\Theta_{2D} = 35$ K, a value in reasonable accord with expectations. Analysis of He films on Grafoil[15] leads to a similar conclusion.

Although Eq. (8) seems to give reasonable estimates of T_m in the few cases where it has been applied, it tells us nothing about the nature of the transition. Kosterlitz and Thouless,[36] using a mean-field theory of dislocation interactions find that the heat capacity and all of its derivatives remain finite at the melting temperature. On the other hand, computer studies of the melting of hard sphere disks appear to indicate a first-order transition.[38]

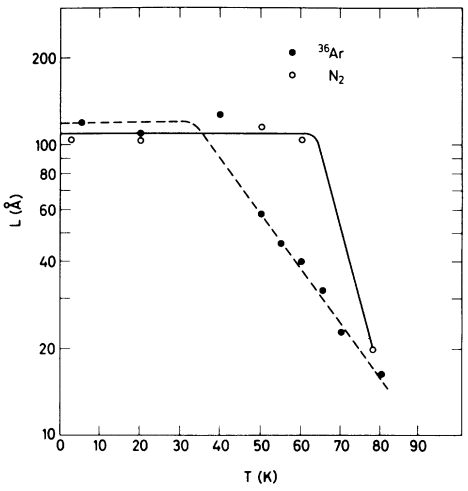

FIG. 7. Temperature variation of the spatial correlation range (or cluster size) in adsorbed Ar and N_2 monolayers. The N_2 monolayer forms a $\sqrt{3} \times \sqrt{3}$ registered phase. Note its greater stability and the abrupt change in correlation range at melting. Ar monolayers do not form a registered phase and the change in correlation range is more gradual. The solid and dashed lines are guides to the eye and have no theoretical significance.

C. Influence of the Ar monolayer on Bragg reflections from the graphite substrate

The presence of overlayers of gas on the basal-plane surfaces of graphite not only produces the characteristic 2D diffraction peaks discussed above but also modifies the $\{00l\}$ Bragg relections from the substrate. To understand the way in which this occurs consider diffraction from the basal planes of a substrate crystallite N layers thick with interplanar spacing d and scattering amplitude b_s per unit area. The elastic scattering from this crystallite will be proportional to

$$I_N(Q_z) \approx \left| \sum_{n=0}^{N-1} b_s \exp(iQ_z nd) \right|^2 = b_s^2 \frac{\sin^2(NQ_z d/2)}{\sin^2(Q_z d/2)} , \tag{9}$$

where Q_z is the projection of the scattering vector $\vec{Q}$ on the c-axis direction. Equation (9) gives a Bragg peak of height proportional to N^2 and width proportional to $1/N$. Adding another layer of carbon atoms at a distance d simply causes the peak height to increase and the width to decrease. The difference between the two diffraction peaks, i.e., $I_{N+1} - I_N$ will therefore be a curve with a narrow central peak and symmetrically placed negative wings. But suppose the added layer consists of a different species of atom sited at a distance $d+\delta$ above the surface. In this case, the total Bragg intensity from the substrate plus adsorbed film will be

$$I_{s+a}(Q_z) \approx \left| b_s \sum_{n=0}^{N-1} \exp(iQ_z nd) + b_a \exp[iQ_z(Nd+\delta)] \right|^2 , \tag{10}$$

where b_a represents the scattering amplitude per unit area of the adsorbed film. Expanding Eq. (10) yields

$$I_{s+a}(Q_z) \approx I_s(Q_z) + b_a^2 + 2b_a b_s \cos[\tfrac{1}{2}(N+1)Q_z d + Q_z \delta] \times \frac{\sin(NQ_z d/2)}{\sin(Q_z d/2)} . \tag{11}$$

The difference $I_{s+a} - I_s$ is no longer symmetric. It now consists of a constant term b_a^2 and, in addition, a term which varies with Q_z and contains information about δ, the amount by which the position of the film differs from the interplanar spacing in the substrate.

At low temperatures the {10} diffraction peak from the Ar film is very close to the {002} substrate reflection and it is difficult to separate one from the other accurately. But at higher temperatures the expansion of the film moves the two peaks far enough apart so that the influence of the interference term becomes evident. This is shown in Fig. 8 where the difference peak for the graphite {002} reflection is plotted. The solid and dashed lines represent best fits of the data to Eq. (11) obtained with $\delta = +0.75$ Å (the distribution of crystallite thicknesses was taken to be Gaussian with a full width of 19 layers and with a mean thickness N of 30 and 25 layers, respectively). It is also possible to estimate the fractional contribution to the intensity from the adsorbed film by comparing the height of the peak in the difference distribution of Fig. 8 to that of the {002} peak from the substrate. We find $I_{s+a} - I_s / I_{002} \approx \frac{1}{20}$ compared with an expected value of about $\frac{1}{40}$. Considering the fact that no corrections were made to take account of such factors as extinction and preferred orientation, the degree of agreement is probably not unreasonable.

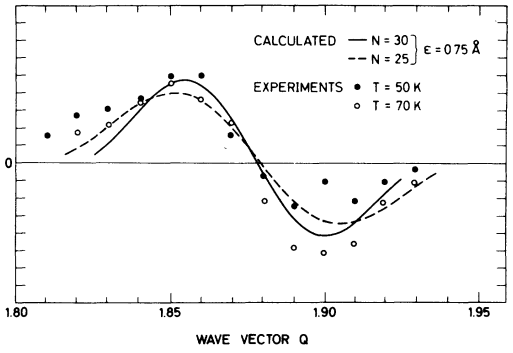

FIG. 8. Difference diffraction pattern in the region where the {002} graphite peak overlaps the {10} peak from the Ar film. The solid and dashed lines are fits of Eq. (11) to the data at 50 and 70 K, respectively, with $\delta = +0.75$ Å.

To complete this discussion, however, we should note that a measurement of this type depends to a degree on knowing the thickness distribution of the substrate crystallites and is very sensitive to slight errors in the positioning of the spectrometer arm, the latter having the effect of distorting the difference distributions in the same way they are distorted by interference from gas overlayers. Since no special precautions were taken to monitor the location of the spectrometer arm, we do not feel that our measurement should be regarded as a definitive determination of the distance between the Ar monolayer and the substrate surface. We make mention of it here only because we believe the method has the potential to provide accurate positional information.[9]

If taken literally, our results suggest that the Ar film is $3.35 + 0.75 = 4.1$ Å above the graphite basal plane at temperatures in the range between 50 and 70 K. This is to be compared with 3.4 Å, the value estimated using a Lennard-Jones 6-12 potential to describe the effective Ar-C interaction.[39] At this time, however, we are not at all certain that the difference as measured ought to be taken seriously.

V. INELASTIC SCATTERING FROM THE ADSORBED ARGON FILMS

A. Experimental observations

Investigating the dynamics of surface monolayers involves the analysis of the energy distribution of neutrons inelastically scattered by the film. Because surface layers contain relatively few atoms and the cross sections for inelastic processes are small, it is usually very difficult to identify their contribution to the scattering. ^{36}Ar, as earlier noted, is an exception in this respect because of its unusually large coherent scattering cross section. This alone would be enough to make it attractive for inelastic neutron scattering studies. However, it also has other favorable characteristics worthy of mention. First, since Ar is a monatomic gas the inelastic spectra will not be complicated by intramolecular transitions. Second, the dynamical response of 3D solid Ar is thoroughly documented[40] and can serve as a guide to the interpretation of 2D spectra. And third, Ar is a noble gas and as such its interactions can be reasonably well represented by simple short-range potentials in which the dis-

tance between atoms is the only variable. Thus the computational complexities of dynamical models involving Ar films can be expected to be much reduced.

Because of its 2D-like character, the dynamical response of an adsorbed monolayer will in general be very anisotropic, i.e., it will vary markedly depending on whether the atomic motions are parallel or perpendicular to the film plane. In this circumstance it would obviously be preferable to work with a 2D single crystal so that the individual components of the scattering could be isolated and separately investigated. Unfortunately, no more than a crude approximation to this is possible with a Grafoil substrate since Grafoil is not a highly ordered material. To take fullest advantage of the orientational order that does exist, we made inelastic scans with three different sample orientations: (i) an in-plane configuration in which the Grafoil sheets were parallel to the scattering plane; (ii) an out-of-plane configuration in which the Grafoil sheets were perpendicular to the scattering plane, and (iii) a 45° configuration intermediate between the two. For reasons having to do with the way neutrons couple to vibrational modes (to be discussed in detail in the following section), in-plane motions contribute more to the scattering in the in-plane configuration and out-of-plane motions in the out-of-plane configuration. It should be kept in mind, however, that in no case is either component of the response completely isolated from the other.

All inelastic scans were made with the scattering vector $\vec{Q}$ held constant and with the sample temperatures fixed within the range between 5 and 80 K. Most involved monolayer films; however, in a few cases the coverage was reduced to $\frac{3}{4}$ or $\frac{1}{2}$ monolayer. We also made some scans at coverages exceeding one monolayer but these will not be discussed here.

As was true of the elastic diffraction measurements, the inelastic scattering from the film was taken to be the difference between counts observed with and without Ar in the cell. Typical experimental spectra are shown at the top of Figs. 9 and 10 representing energy-loss scattering from ^{36}Ar monolayers at a temperature of 5 K observed in the in-plane and out-of-plane geometries respectively. It is evident from the figures that regardless of either the cell orientation or the value of Q two reasonably well-defined peaks appear at energy transfers near 3 and 5.5 MeV. The relative intensities of the peaks is seen, however, to depend

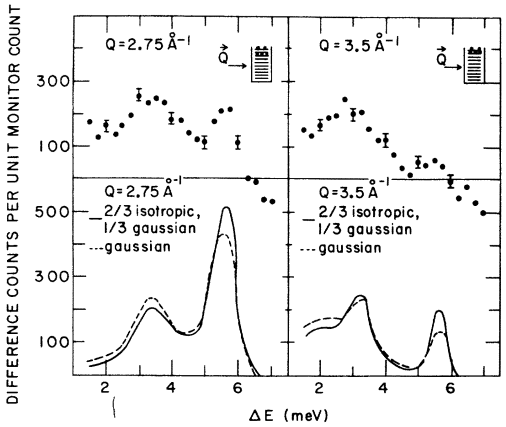

FIG. 9. Inelastic spectra from Ar monolayers at 5 K observed with the scattering vector $\vec{Q}$ parallel to the plane of the graphite foils. The solid circles at the top are experimental difference data. Plotted below are spectra computed using Eqs. (12) and (15) assuming a partly-ordered–partly-isotropic orientational distribution (solid line) and a distribution with only the partly ordered component (dashed line). Comparison of the dashed and solid curves gives an indication of the influence of orientational order on the experimental spectra.

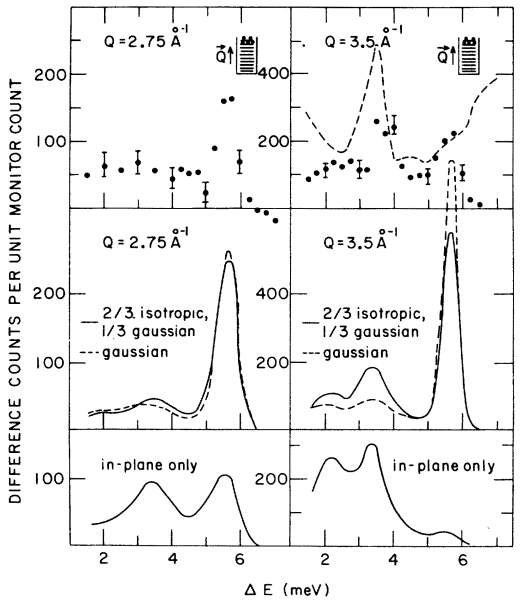

FIG. 10. Inelastic spectra from Ar monolayers at 5 K observed with the scattering vector $\vec{Q}$ normal to the plane of the graphite foils. The solid circles at the top are experimental difference data; the dashed line represents the inelastic background with only Grafoil in the cell. Plotted underneath are spectra computed using Eqs. (12) and (15) assuming a partly-ordered–partly-isotropic orientational distribution (solid line) and a distribution with only the partly ordered component (dashed line). The curves at the bottom represent the calculated contribution to the observed spectra due to in-plane scattering from misoriented crystallites.

markedly on the value of Q. For example, in the out-of-plane configuration of Fig. 10 very little intensity is observed near 3 MeV at $Q = 2.75$ Å^{-1} whereas two peaks with comparable intensity appear when $Q = 3.5$ Å^{-1}. Furthermore, for the same value of Q the relative intensities change dramatically as the cell is tilted. When submonolayer films were studied the same basic results were obtained but the intensities were smaller in proportion to the reduced coverage.

B. Interpretation of the low-temperature spectra

It is evident from the foregoing that both the neutron-phonon interaction cross section and the orientational distribution of the surface films are important elements in determining the shape of the inelastic spectra. In due course we will want to examine the role of each in detail. But before doing so let us first take an overall look at what will be involved in this analysis. Suppose, for example, that the sample under investigation was not polycrystalline but consisted of a 2D single crystal. In this case the spectrum would consist of well-defined peaks associated with discrete phonons propagating in specific directions in the 2D lattice. On the other hand, if the sample was polycrystalline and the wave vector transfer $Q \gg 2\pi/a$, the spectra would then be more nearly representations of the density of phonon states. Unfortunately, the experimental constraints are such that we are at neither one limit nor the other but somewhere in between. As a result we are obliged to model the coherent dynamic structure factor $S_{\text{coh}}(\vec{Q}, \omega)$, perform the appropriate orientational averaging on a computer and see if we can duplicate the experimental observations. We found that relatively simple models reproduce the observed spectra reasonably well. From these model computations, as we will soon show, we are able to establish with some certainty that the two peaks observed in the in-plane configuration of Fig. 9 are associated with longitudinal and transverse zone boundary phonons polarized and propagating in the 2D film planes. We are also able to show (with somewhat less certainty) that the extra contribution to the scattering observed in the out-of-plane configuration of Fig. 10 is identified with atomic motions normal to the film planes.

Our first step in modeling the dynamics of the Ar film was to make the assumption that atomic motions parallel to the substrate surface are not strongly coupled to perpendicular motions and therefore each could be treated separately. Since the elastic diffraction data indicate that the Ar monolayers form ordered structures, a natural starting point for interpretation of the in-plane component of the inelastic scattering is to assume that it represents the collective excitations of a 2D solid. To describe the one-phonon dynamic structure factor of these in-plane modes we took the expression[41]

$$[S_{\text{coh}}(\vec{Q}, \omega)]_{\text{poly}} = \exp(-2W)[n(\omega)+1](\hbar Q^2/2M\omega) \times \left\langle \sum_{j=1}^{2} [\hat{Q} \cdot \hat{c}_j(\vec{q})]^2 \delta(\omega - \omega_j(\vec{q})) \right\rangle , \tag{12}$$

an equation of the same basic form as that used by de Wette and Rahman[42] to calculate the inelastic scattering from 3D fcc polycrystals but modified to apply to the 2D case. In Eq. (12), $\exp(-2W)$ represents the in-plane Debye-Waller factor, $n(\omega)$ is the phonon occupation number $[\exp(\hbar\omega k_B T) - 1]^{-1}$, M the ^{36}Ar mass, $\hat{Q}$ a unit vector directed along the scattering vector $\vec{Q}$ and the $\hat{c}_j(\vec{q})$'s are the orthonormal phonon eigenvectors associated with the phonon eigenfrequencies $\omega_j(\vec{q})$. The angular brackets imply an averaging of $\vec{Q}$ over all appropriate orientations.

For the in-plane Debye-Waller factor we used the value $\langle u^2 \rangle = \langle u_x^2 \rangle + \langle u_y^2 \rangle = 0.08$ Å^2 estimated from the elastic diffraction measurements discussed in Sec. IV A. The eigenvectors and eigenfrequencies were calculated in the Born–von Kármán approximation assuming a 2D triangular lattice and using a Lennard-Jones potential of the form

$$V(r) = 4\epsilon[(\sigma/r)^{12} - (\sigma/r)^6] \tag{13}$$

to represent the interaction between Ar atoms. The constants ϵ and σ were assigned the values 10.3 MeV and 3.40 Å, respectively, obtained from virial coefficient studies of the gas phase.[31] Interactions between the adsorbed film and the substrate were assumed to have little influence on the modes in question and were therefore neglected.

The phonon dispersion curves computed for the principal symmetry directions of the 2D Ar reciprocal lattice are plotted in the bottom half of Fig. 11. Figure 12 shows the computed density of phonon states $g(E)$. Note that $g(E)$ varies linearly with E for small values of E—a consequence of the 2D character of the system.

Calculation of the contribution of the in-plane modes to the inelastic scattering requires the angular averaging of Eq. (12). This was done in the following way: A crystalline tilt angle γ was chosen at random in accordance with the orientational distribution function $H(\gamma)$ defined by Eq. (1).[43] With this value of γ, the projection of the scattering vector on the film plane, i.e., $Q\cos\gamma$ was calculated and then substituted for Q in Eq. (12) with an azimuthal orientation chosen at random along a 30° arc

in reciprocal space. Examples of such arcs (which span the irreducible part of the 2D Brillouin zone) are shown in the top half of Fig. 11 for $Q\cos\gamma = 2.2$, 2.75, and 3.5 Å^{-1}. The process was repeated until the accumulated statistics indicated a stable distribution had been formed.

Thus far we have only considered atomic motions parallel to the film plane. Part of the dynamical response is, however, associated with perpendicular motions and these modes can also be expected to contribute to the inelastic scattering, particularly when $\vec{Q}$ is oriented normal to the foil planes. In the Appendix we have argued that the out-of-plane motions are not localized, Einstein-like oscillations but rather resonant modes coupled to both longitudinal phonons of the substrate propagating normal to the basal planes and to transverse modes of the substrate propagating in the basal planes but with polarizations normal to the surface.[44] Even so, according to our analysis much of the weight of the out-of-plane response is concentrated near the Einstein energy, i.e., between 5 and 6 MeV, which, as it happens, falls within the same energy range as the bulk of the response from in-plane, longitudinal modes. Considering that the out-of-plane response appears to be concentrated at the Einstein oscillator energy (5.6 MeV) we felt that it would be a reasonable approximation in our model to take the out-of-plane scattering to be represented by a set of Einstein oscillators with a distribution of energies centered around 5.6 MeV. In this case, if we restrict ourselves to neutron-energy-loss processes and consider only transitions involving transfer of single units of energy $\hbar\omega_0$, the appropriate form of the dynamic structure factor is[41]

$$S_{\mathrm{coh}}(\vec{Q},\omega) = \exp\left(-\frac{\hbar Q^2}{2M\omega_0}\coth\frac{\hbar\omega_0}{2k_BT}\right)\exp(\hbar\omega/2k_BT) \times I_1\left(\frac{\hbar Q^2}{2M\omega_0}\,\mathrm{cosech}\,\frac{\hbar\omega_0}{2k_BT}\right)\delta(\hbar\omega-\hbar\omega_0)\,, \tag{14}$$

where $\hbar\omega_0$ is the oscillator energy and I_1 a modified Bessel function of the first kind. It is shown in Ref. 41 that in the limit when Q^{-1} is large compared to the amplitude of vibration, Eq. (14) reduces to the simpler form

$$S_{\mathrm{coh}}(\vec{Q},\omega) = \exp[-2W(Q)][n(\omega_0)+1] \times (\hbar Q^2/2M\omega_0)\delta(\hbar\omega-\hbar\omega_0), \tag{15}$$

which is similar to Eq. (12) as would be expected. Thus for each crystallite tilt angle γ selected, the out-of-plane contribution to the inelastic scattering was computed by substituting for Q in Eq. (14) the value of its projection on the normal to the film plane—i.e., $Q\sin\gamma$—and taking a weighted average over a Gaussian distribution of oscillator energies with a half-width of 0.35 meV centered at 5.6 meV.

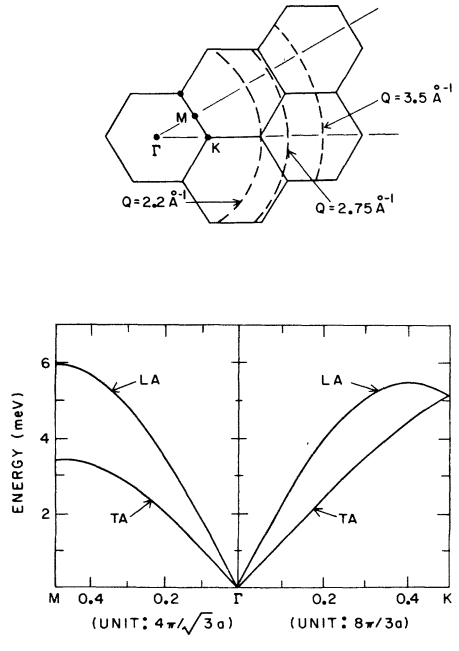

FIG. 11. At the top: the region of reciprocal space covered by the in-plane scans of Fig. 9. Underneath: dispersion curves for principal symmetry directions of an isolated 2D triangular Ar lattice calculated assuming the atoms to be coupled by the standard Lennard-Jones Ar-Ar interaction potential. The Lennard-Jones parameters are given in Sec. V B of the text.

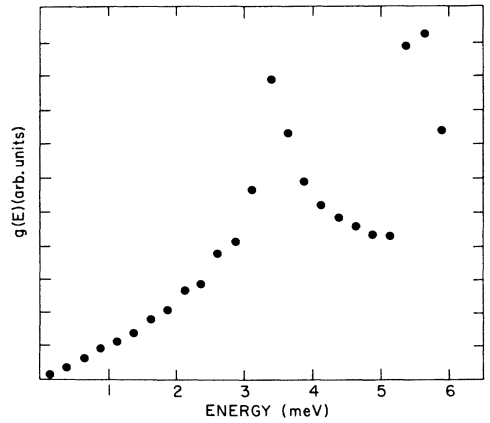

FIG. 12. Density of phonon states of an isolated 2D triangular Ar lattice calculated assuming the atoms to be coupled by the standard Lennard-Jones Ar-Ar interaction potential. The Lennard-Jones parameters are given in Sec. V B of the text. Note the peaks at 3.5 and 5.5 MeV.

One further point ought to be noted. Before making direct comparisons with the observed spectra the distributions calculated using Eqs. (12) and (15) were folded with the instrumental energy resolution function and weighted to take into account the decrease in spectrometer efficiency with increasing energy transfer.

The spectral distribution computed for each value of Q and each orientation of the sample cell is plotted beneath the corresponding observed spectrum. To indicate how much the results are influenced by orientational effects, the computations were first made with the orientational distribution derived from our studies of adsorbed N_2 (two-thirds isotropic and one-third Gaussian) and then repeated without the isotropic component. The resulting spectra appear as solid and dashed lines, respectively. In addition, where the relative weight of the in-plane and out-of-plane contributions to the scattering is of interest, we have also plotted the in-plane component separately.

Considering first the predominantly in-plane spectra of Fig. 9, we note that not only are they reasonably well represented by the computed spectra but even the shift in spectral weight with changing Q is satisfactorily reproduced. The computations make it clear that the peaks at 3 and 5.5 meV are related to the zone boundary energies of the in-plane modes. A little thought shows that they appear for two reasons: (i) the largest part of the scattering originates from regions of reciprocal space near zone boundaries where the density of phonon states is high, and (ii) the relative weight of the contribution from transverse and longitudinal modes is governed by the term $[\hat{Q}\cdot\hat{c}_j(\vec{q})]^2$ in Eq. (12). It is easy to see from Fig. 11 that when $Q = 3.5$ Å^{-1} the phonon-propagation vector $\vec{q} = \vec{Q} - \vec{\tau}$ is nearly perpendicular to $\vec{Q}$ at the zone boundary ($\vec{\tau}$ is the reciprocal lattice vector from the origin to the zone center). Therefore, in this case, the greatest part of the response comes from transverse modes with energies in the neighborhood of 3 meV. On the other hand, when $Q = 2.75$ Å^{-1} the phonon propagation vectors near the zone boundary form an intermediate angle with $\vec{Q}$ and as a consequence part of the response comes from transverse modes with energies near 3 meV and the rest from longitudinal modes with energies falling primarily between 5 and 6 meV.

Turning to the predominantly out-of-plane configuration of Fig. 10, we note that here too the spectra are well represented by our computer simulations, particularly when an out-of-plane response is included in the analysis. The only obvious problem is at $Q = 3.5$ Å^{-1} where the relative weights of the high- and low-energy peaks are not correctly predicted.

In the 45° geometry of Fig. 13 it is evident that the computer simulations underestimate the weight of the low-energy peak (particularly at $Q = 2.75$ Å^{-1}) when the out-of-plane response is included. Although we cannot prove it, we suspect that neglecting to take account of coupling between in-plane and out-of-plane modes is responsible for most of the differences between the observed and computed spectra. It would be interesting to investigate this question further but unfortunately such experiments require far better oriented substrates than are available at the present time.

The foregoing analysis, although oversimplified, nevertheless provides a number of interesting insights into the dynamical properties of the film. First, and probably most important, we see that in-plane modes of the Ar monolayer are little influenced by the substrate and can be described remarkably well by a simple 2D harmonic phonon model incorporating nearest-neighbor Ar-Ar force constants as derived from studies of the gas phase. Both this and the fact that the films form as nonregistered structures are obviously consequences of the relatively strong coupling between Ar atoms

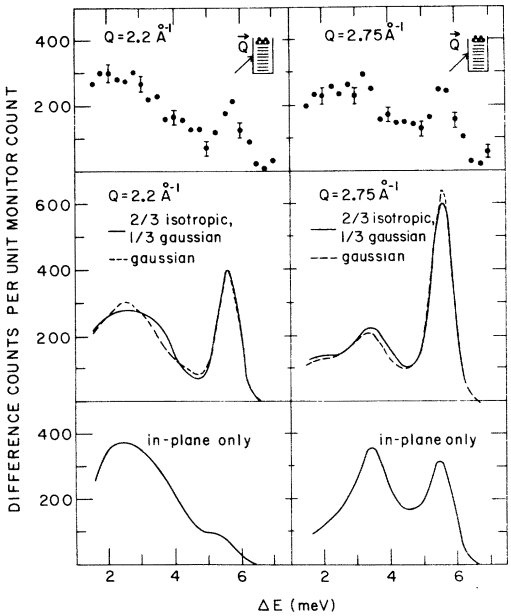

FIG. 13. Inelastic spectra from Ar monolayers at 5 K observed with scattering vector $\vec{Q}$ at a 45° angle to the plane of the graphite foils. The solid circles at the top are experimental difference data. Plotted underneath are spectra computed using Eqs. (12) and (15) assuming a partly-ordered–partly-isotropic orientational distribution (solid line) and a distribution with only the partly ordered component (dashed line). The curves at the bottom represent the calculated contribution to the observed spectra due to in-plane scattering from misoriented crystallites.

and the unusual smoothness of the graphite surface potential; or, to state it in another way, of the fact that the Ar-Ar bond is much stronger than the variation of the Ar-C interaction from point to point on the graphite basal-plane surfaces.[45] No doubt the effective surface potential for dynamical processes is further smoothed by the incommensurability of the film and substrate structures since for each atom of the film moving to a more tightly bound position there must be another, on average, doing the opposite.

We can also see from our analysis that the out-of-plane dynamics is primarily associated with modes having energies in the neighborhood of 5 to 6 meV. This is consistent with—but does not prove—resonant coupling of the out-of-plane motions of the film to bulk modes of the substrate as described in the Appendix. Unfortunately, the data do not permit us to make a definitive choice between resonant coupling and a localized, Einstein-like out-of-plane response. (More will be said about this in the Appendix.)

As a check on the internal consistency of our analysis, it is of interest to compare the Debye-Waller factor calculated from the 2D density of phonon states of Fig. 12 with the value derived from the elastic diffraction measurements described in Sec. IV A. Assuming as before a 2D harmonic phonon model, the in-plane Debye-Waller can be calculated from the expression

$$2W_{2D} = \tfrac{1}{2} Q^2 \langle u^2 \rangle_{2D} = \frac{\hbar Q^2}{2M} \int_{\omega_{min}}^{\omega_{max}} d\omega \, \frac{Z(\omega)}{\omega} [2n(\omega) + 1] , \tag{16}$$

where $Z(\omega)$ is the density of in-plane phonon states (i.e., modes with polarizations in the film plane) expressed in frequency units. The lower limit of integration ω_{min} is introduced because of the finite size of the crystallites. We take it to be that of phonons at $q \sim 2\pi/L$, where $L \sim 100$ Å (the exact value chosen has little effect on the result). Integration of Eq. (16) gives $\langle u^2 \rangle_{2D} = \langle u_x^2 \rangle + \langle u_y^2 \rangle = 2\langle u_x^2 \rangle \approx 0.04$ Å^2 at $T = 4.5$ K, i.e., about half the value derived from the diffraction data. Similarly the out-of-plane contribution $\langle u^2 \rangle_\perp$ is found to be ~ 0.01 Å^2 hence $\langle u^2 \rangle_{3D} = \langle u^2 \rangle_{2D} + \langle u^2 \rangle_\perp \sim 0.05$ Å^2. Estimates of the *static* strains induced by the incommensurate substrate potential show them to be of the same order of magnitude.[46] Consequently there are reasons to believe that the comparatively large Debye-Waller factor observed experimentally is as much an indication of static strains in the films as of dynamic displacements.

For completeness we should also mention that there is another way to relate the inelastic spectra to the elastically scattered intensities; namely by the application of the so-called ACB (Ambegaokar-Conway-Baym) sum rule,[47] a useful approach in cases where the inelastic scattering can be identified with well defined values of Q. Unfortunately, in our case even though the measurements were made with a fixed nominal Q, the actual value of Q for scattering from a given 2D crystallite is not the nominal value but rather its projection on the crystallite plane. Consequently our inelastic spectra represent orientationally weighted distributions over values of Q extending from effectively $Q = 0$ to the nominal value, a circumstance in which the ACB sum rule cannot be easily applied.

C. Temperature dependence of the spectra

Let us now turn to consideration of the temperature dependence of the dynamical response. On the left-hand side of Fig. 14 we show spectra observed in the in-plane configuration with $Q = 3.5$ Å^{-1} at temperatures ranging from 5 to 80 K. One can see that the spectra evolve smoothly from a typical 2D solid response at the lowest temperature to something not unlike that of a classical bulk liquid at $T = 80$ K. Note that there is no abrupt signature of melting.

Part of the spectral shift observable in the figure arises simply from the phonon population factor $n(\omega) + 1$ in the cross section; the rest is due to changes in the density of phonon states. To separate these two effects, we have reduced the data

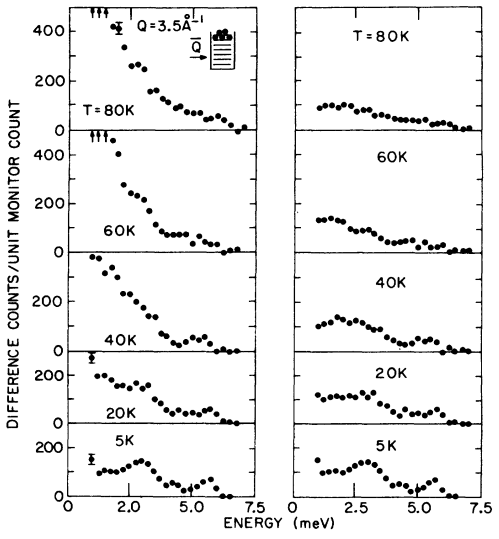

FIG. 14. On the left: the temperature dependence of in-plane spectra from Ar monolayers at $Q = 3.5$ Å^{-1}. On the right: the temperature dependence of the nominal "density of phonon states" obtained by dividing the observed spectra by the phonon population factor $[n(\omega) + 1]$.

of Fig. 14 to an "effective density of states" $Z(Q,\omega,T)$ defined as $S(Q,\omega)/[n(\omega)+1]$. The result appears on the right hand side of Fig. 14. Both of the peaks characteristic of the 2D solid are identifiable up to $T\sim 40$ K; at this temperature the high frequency longitudinal mode appears to renormalize slightly, shifting from roughly 5.8 to 5.3 meV, while the low-frequency transverse peak seems to renormalize relatively much more, going from about 3 to 2 meV. It is interesting to see that the transverse modes soften as the film approaches the "melting region" $40 \lesssim T \lesssim 60$ K. Outside this retion, in the temperature range between 60 and 80 K, $Z(Q,\omega,T)$ no longer shows any well-defined structure. In this case the in-plane modes evidently become over-damped as is also true of classical liquids.

Interestingly, the temperature dependence of the out-of-plane response is quite different. Scans made over the same temperature range in the out-of-plane geometry with $Q=2.75$ Å^{-1} are shown on the left-hand side of Fig. 15. Even at 80 K the resonant mode at 5.6 meV can still be identified although it is considerably broadened and somewhat lower in energy. The corresponding "density of states" is plotted on the right-hand side of the figure. Although the high-frequency part of $Z(Q,\omega,T)$ appears to be roughly temperature independent, the weight of the low frequency part is seen to increase as the temperature is raised, at least up to 61 K. (Why this occurs is not known. It may possibly be a result of surface roughening, i.e., promotion of first-layer atoms to a second layer.) Finally, we note that above 61 K the overall scattered intensity decreases slightly, presumably due to partial desorption of the film.

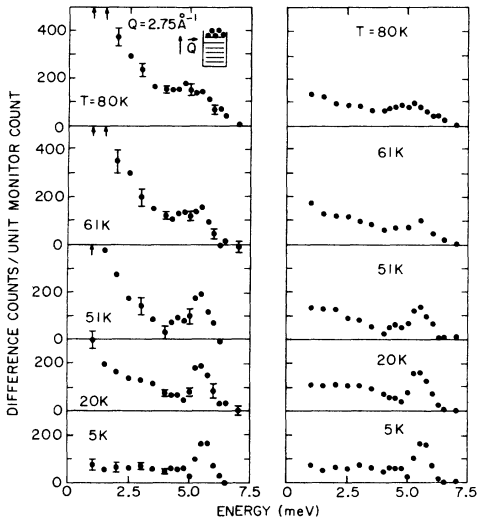

FIG. 15. On the left: the temperature dependence of the out-of-plane spectra from Ar monolayers at $Q=2.75$ Å^{-1}. On the right: the temperature dependence of the nominal "density of states" obtained by dividing the observed spectra by the phonon population factor $[n(\omega)+1]$.

VI. DISCUSSION

Certainly the most striking feature of the Ar monolayers we have been studying is the degree to which they behave as 2D entities. We have seen this manifest itself in a variety of ways: in the fact that the structure of the overlayer is incommensurate with the substrate, in the apparently continuous melting of the low-temperature solid phase, in its anomalously large thermal expansion and in the nature of its in-plane dynamical response. Taken together, these observations make a strong case for the 2D-like character of the film.

At the same time it is also clear from our experiments that a 2D description of surface monolayers is not without its limitations. Unlike idealized 2D systems, the atoms of the film are not constrained to move in the film plane alone. The effects of this are obvious in both the distinctive out-of-plane contribution to the dynamical response and in the evidence of layer promotion at higher temperatures. Furthermore, although graphite basal planes are remarkably uniform, they are not, even at our level of sensitivity, ideally smooth surfaces. In fact, our experiments suggest that the incommensurate periodic potential of the substrate produces static in-plane strains of considerable magnitude in the adsorbed films. No doubt the incommensurability of the two structures also produces equivalent static displacements in the out-of plane direction and it would be surprising if these did not have the effect of coupling the in-plane and out-of-plane components of the dynamical response. In fact it is likely that the limitations of our dynamical computations stem at least as much from neglect of this factor as from other considerations.

ACKNOWLEDGMENTS

We are grateful to Dr. A. D. Novaco for many helpful discussions of surface monolayer theory. We also wish to express our appreciation to Dr. J. G. Dash and his co-workers for advice and help with the preparation of the Grafoil substrate.

APPENDIX

The concept of coupling between the out-of-plane motions of the Ar overlayer and the collective modes of the graphite substrate is most easily understood by considering the dynamical response of a one-dimensional analog of the film-substrate sys-

tem, namely a linear chain of light atoms with a heavy atom attached to one end of the chain. In this model we need only deal with longitudinal collective modes because these are the equivalent of the out-of-plane modes of the 2D system in which we are interested. It should be kept in mind, however, that in a real adsorbed phase system transverse modes of the substrate with polarization vectors in "out-of-surface" directions will also couple to the surface film.[48]

First, let us consider briefly the justification for taking a coupled-system approach to the out-of-plane dynamics. As a rough estimate of the energies associated with out-of-plane motions of the surface film, we take the Einstein oscillator energy of an Ar atom vibrating against a rigid C substrate. This can be estimated from the Ar-C force constant[39] and is found to be about 5.6 meV. Concerning the collective excitations of the substrate, neutron scattering experiments[49] indicate that the energies of longitudinal graphite modes propagating in the c-axis direction extend up to 16.5 meV. Thus the energies of the out-of-plane Ar motions fall within the band defined by the longitudinal substrate modes and coupling between the two types of excitations is almost certain to occur, the atoms of the film acting in effect like massive impurities in a host crystal composed of light atoms. (This argument does not, of course, apply to in-plane motions because the film is incommensurate with the substrate.)

The model we considered consisted of a chain of 30 light atoms (representing a typical set of graphite basal planes) with a heavy atom (representing the Ar monolayer) at one end. To make it as realistic as possible, the C-C force constant along the chain was chosen so as to reproduce the dispersion curve of graphite for longitudinal modes propagating in the c-axis direction and the Ar-C force constant was modified to take account of the lower number density in the surface film. In addition, the masses of the light and heavy atoms on the chain were adjusted so that they represented the average areal density in the graphite basal planes and in the Ar overlayer respectively.

The inset to Fig. 16 shows examples of typical eigenvectors predicted by the model. The calculated relative displacements of the heavy atoms as a function of mode energy are plotted in the main part of the figure. It is evident from the latter that the response is strongly resonant, centering at the Einstein oscillator energy, i.e., at about 5.6 meV. Furthermore, although the motion of the heavy atom at the end of the chain is coupled to that of the light atoms, displacement of the heavy atom is much greater in the resonance region and is in fact not very different from what it would have been if

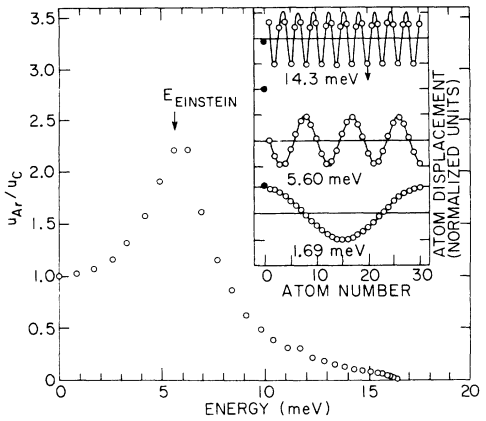

FIG. 16. (a) The calculated relative longitudinal displacement of an Ar atom at the end of a one-dimensional chain of 30 C atoms as a function of the excitation energy of the chain. Note the resonant response in the neighborhood of the Einstein oscillator energy (5.6 meV). (b) Inset: calculated eigenvectors for low-, medium-, and high-frequency modes of the chain. Atom number 0 is the Ar atom at the end of the chain; the solid circle represents its displacement while the open circles are the C atom displacements. It is evident that the Ar atom follows the low-frequency motions of chain; however, because of its mass, it is unable to respond at higher frequencies. At the Einstein oscillator energy (5.6 meV) the calculations indicate the Ar atom displacements are anomalously large.

the atom had been coupled to a rigid rather than a moving surface. As a result the dynamical response will be very much like that of the equivalent Einstein oscillator although somewhat spread out in energy.

Another interesting aspect of the dynamical coupling between film and substrate is that it is expected to produce an enhancement of the neutron response to resonant modes of the substrate. To see the reason for this, consider the coherent dynamic-structure factor describing the inelastic scattering process. For modes propagating normal to the substrate basal planes, this quantity can be written in the form

$$S(Q,\omega)=\sum_j\left|\sum_{l=0}^{N-1} b_l(\vec{\mathbf{Q}}\cdot\vec{u}_l^j)\exp(i\vec{\mathbf{Q}}\cdot\vec{\mathbf{R}}_l)\right|^2\delta(\hbar\omega-\hbar\omega_j)\,, \tag{A1}$$

where j is a mode index, b_l is the scattering length per unit area of the lth atomic plane and u_l^j is the amplitude of the eigenvector of the jth mode of this plane. (The Debye-Waller factor has been neglected in the interest of simplicity.) To model the film on the substrate we take the $l=0$ layer to be the film and identify all values of $l>0$ with substrate planes. In addition, to further simplify the computation we assume all scattering lengths to be identical. In this case Eq. (A1) ultimately reduces to

$$S(Q,\omega) = bb^* \sum_j \delta(\hbar\omega - \hbar\omega_j) \times \left(|\vec{Q}\cdot\vec{u}_0^j|^2 + \vec{Q}\cdot\vec{u}_0^j \sum_{l\neq 0} [\vec{Q}\cdot\vec{u}_l^j \exp(i\vec{Q}\cdot\vec{R}_l) + \text{c.c.}] + \left| \sum_{l\neq 0} \vec{Q}\cdot\vec{u}_l^j \exp(i\vec{Q}\cdot\vec{R}_l) \right|^2 \right), \quad \text{(A2)}$$

where c.c. denotes the complex conjugate. The first term represents the "Einstein oscillatorlike" response which is peaked sharply at the resonant frequencies where the displacement u_0 is large compared to the u_l's, while the last term is the response of the substrate in the absence of the overlayer (assuming there are no frequency shifts due to the presence of the film). The second term produces a Q-dependent enhancement of the bulk modes. Since u_0 falls off rapidly above the resonance region, it is evident that only substrate modes near resonance will be significantly enhanced by the presence of the film.

An attempt was made to detect this effect by looking carefully at the out-of-plane response of the film at values of Q between 3.5 and 3.6 Å^{-1}, i.e., within the wave vector range in which the substrate scattering comes primarily from longitudinal graphite phonons with energies between 5 and 6 meV propagating along the c-axis direction. We estimated that resonant coupling would increase the intensity of scattering from the film by about 4% near $Q = 3.55$ Å^{-1} where the graphite longitudinal-mode frequency closely matches the Einstein frequency of the film. A small increase was observed but unfortunately the statistical scatter in the data was too large to regard it as significant. Therefore, as the matter now stands we are unable to provide unequivocal experimental evidence of resonant coupling although we believe it offers a physically plausible description of our experimental observations.

*Present address: Physics Dept., University of Missouri, Columbia, Mo. 65201.
†Guest Scientist at Brookhaven National Laboratory. Present address: Phys. Laboratory I, H. C. Oersted Institute, D. K. 2100, Copenhagen Ø, Denmark.
‡Guest Scientist at Brookhaven National Laboratory. Present address: Research Establishment Risø, DK 4000, Roskilde, Denmark.
§Work performed under the auspices of the U.S. ERDA.
¶Supported in part by the John Simon Guggenheim Foundation and by NSF.

[1]A comprehensive review of methods for physisorption studies is given in *Films on Solid Surfaces*, J. G. Dash (Academic, New York, 1975).
[2]J. K. Kjems, L. Passell, H. Taub, J. G. Dash, and A. D. Novaco, Phys. Rev. B 13, 1446 (1976).
[3]H. Taub, L. Passell, J. K. Kjems, K. Carneiro, J. P. McTague, and J. G. Dash, Phys. Rev. Lett. 34, 654 (1975).
[4]K. Carneiro, W. D. Ellenson, L. Passell, J. P. McTague, and H. Taub, Phys. Rev. Lett. 37, 1695 (1976).
[5]Grafoil is the trademark of an expanded graphite product marketed by the Union Carbide Corp., Carbon Products Div., 270 Park Ave., New York, N. Y. 10017.
[6]M. Nielsen, W. D. Ellenson, S. M. Shapiro, and K. Carneiro, *Low Temperature Physics* (Academy of Sciences, Ukrainian SSR, 1975), Vol. 1, No. 6.
[7]M. Nielsen and W. D. Ellenson, (unpublished).
[8]J. P. McTague and M. Nielsen, Phys. Rev. Lett. 37, 596 (1976).
[9]P. Thorel, B. Croset, C. Marti and J. P. Coulomb, Proceedings of the Conference on Neutron Scattering, Gatlinburg, Tenn., edited by R. M. Moon, pg. 85 (1976) (Oak Ridge National Laboratory Report No. CONF-760601) (unpublished).
[10]H. Boutin, G. J. Safford, and H. R. Danner, J. Chem. Phys. 40, 2670 (1964).
[11]G. Verdan, Helv. Phys. Acta 41, 533 (1968).
[12]S. Todireanu and S. Hautecler, Phys. Lett. A43, 189 (1973).
[13]R. Stockmeyer, H. M. Conrad, A. Renouprez, and P. Fouilloux, Surf. Sci. 49, 549 (1975).
[14]M. Bretz, J. G. Dash, D. C. Hickernell, E. O. McLean, and O. E. Vilches, Phys. Rev. A 8, 1589 (1973).
[15]R. L. Elgin and D. L. Goodstein, Phys. Rev. A 9, 2657 (1974).
[16]F. A. Putnam and T. Fort, Jr., J. Phys. Chem. 79, 459 (1975).
[17]A. Thomy and X. Duval, J. Chem. Phys. 67, 1101 (1970).
[18]J. Suzanne, J. P. Coulomb, and M. Bienfait, Surf. Sci. 40, 414 (1973).
[19]E. Lerner and J. G. Daunt, J. Low Temp. Phys. 10, 299 (1973).
[20]R. J. Bobka, R. E. Dininny, A. R. Siebert, and E. L. Pace, J. Phys. Chem. 61, 164 (1957).
[21]W. A. Steele and R. Karl, J. Colloid Interface Sci. 28, 397 (1968).
[22]For a general discussion of electron spectroscopic methods for surface studies see for example J. T. Yates, Jr., Chem. Eng. News 52, No. 34, 19 (1974).
[23]H. H. Farrell, M. Strongin, and J. M. Dickey, Phys. Rev. B 6, 4703 (1972).
[24]J. J. Lander and J. Morrison, Surf. Sci. 6, 1 (1967).
[25]J. Suzanne, J. P. Coulomb, and M. Bienfait, Surf. Sci. 44, 141 (1974).
[26]J. P. Coulomb, J. Suzanne, M. Bienfait, and P. Masri,

Solid State Commun. 15, 1585 (1974).
[27]D. L. Husa, D. C. Hickernell, and J. E. Piott, *Monolayer and Submonolayer Helium Films*, edited by J. G. Daunt and E. Lerner (Plenum, New York, 1973), p. 133.
[28]R. J. Rollefson, *Monolayer and Submonolayer Helium Films*, edited by J. G. Daunt and E. Lerner (Plenum, New York, 1973), p. 115.
[29]B. P. Cowan, M. G. Richards, A. L. Thomson, and W. J. Mullin, Phys. Rev. Lett. 38, 165 (1977).
[30]B. E. Warren, Phys. Rev. 59, 693 (1941).
[31]J. O. Hirschfelder, C. F. Curtiss, and R. B. Bird, *Molecular Theory of Gases and Liquids* (Wiley, New York, 1954).
[32]This value is changed by about 1% when zero-point motion and interactions between other than nearest neighbors are taken into account.
[33]R. E. Peierls, Ann. Inst. Henri Poincare 5, 177 (1935).
[34]N. D. Mermin, Phys. Rev. 176, 250 (1968). Mermin shows that although long-range positional order is ruled out, there can still be long-range "orientational" order in 2D systems, i.e., $\langle \vec{l}_1 \cdot \vec{l}_N \rangle$ can remain finite as $N \to \infty$.
[35]For a detailed discussion of this interesting question, see Y. Imry and L. Gunther, Phys. Rev. B 3, 3939 (1971).
[36]J. M. Kosterlitz and D. J. Thouless, J. Phys. C 6, 1181 (1973).
[37]R. M. Cotterill, E. J. Jensen, and W. D. Kristensen, *Anharmonic Lattices, Structural Transitions and Melting*, edited by T. Riste (Nordhoof International, Leiden, 1974), p. 405.
[38]B. J. Alder and T. E. Wainwright, Phys. Rev. 127, 359 (1962).
[39]W. A. Steele, Surf. Sci. 36, 317 (1973).
[40]Y. Fujii, N. A. Lurie, R. Pynn, and G. Shirane, Phys. Rev. B 10, 3647 (1974).
[41]W. Marshall and S. W. Lovesey, *Theory of Thermal Neutron Scattering*, (Oxford U. P., London, 1971). Equation (12) can be found on p. 91, Eq. (14) on p. 452.
[42]F. W. de Wette and A. Rahman, Phys. Rev. 176, 784 (1968).
[43]Two thirds of the choices were made at random within the range $\frac{1}{2}\pi \leq \gamma \leq \frac{1}{2}\pi$; the other third were selected randomly from a Gaussian distribution with standard deviation 12.7° centered at $\gamma = 0°$.
[44]Neutrons scattering in the film plane do not couple directly to transverse modes of the film propagating in the same plane with polarization vectors directed normal to the film surface.
[45]A discussion of the conditions leading to an incommensurate structure and the influence of incommensurability on the in-plane dynamics of the film can be found in S. C. Ying, Phys. Rev. B 3, 41660 (1971).
[46]A. D. Novaco and J. P. McTague (unpublished).
[47]V. Ambegaokar, J. M. Conway and G. Baym, *Lattice Dynamics*, edited by R. F. Wallis (Pergamon, New York, 1968), p. 261.
[48]A more general treatment of the problem has been made by A. D. Novaco: His results, briefly summarized in Bull. Amer. Phys. Soc. 21, 765 (1976), show that our one-dimensional analog illustrates the most important features of the dynamical response.
[49]R. Nicklow, N. Wakabayashi, and H. G. Smith, Phys. Rev. B 5, 4951 (1972).